Dynamics of the Collinear One-Bumper Two-Body Problem

Samuel R. Kaplan

Department of Mathematics, Bowdoin College, Brunswick, Maine 04011

1. INTRODUCTION

The problem presented in this paper is a model related to the collinear

tion. The three-body problem has been known since Newton to be notoriously difficult. The search for a full solution has motivated a great deal of work but was unsuccessful due in part to the possibility of chaotic behavior discovered by Poincaré in the 1880's and 1890's [3].

The cause of complicated behavior in the three-body problem lay in the fact that solutions can pass near triple collision. In 1974 R. McGehee introduced a transformation which allowed him to extend the phase space to triple collision in the collinear three-body problem. McGehee studied the flow on the collision manifold in some detail in order to understand orbits which pass near to triple collision [1]. His analysis is essentially a tool for understanding systems containing triple collisions.

In 1994, Meyer and Wang showed that the structure of the stable manifold for triple-collision in the phase space of the collinear three-body problem is complicated [2]. They also show the existence of symbolic systems which describe the dynamics but to state the symbolic dynamics requires tracking the stable manifold for triple-collision between binary collisions, a notorious problem at best.

In an effort to study the global effect on the dynamics of the collinear three-body problem due to the existence of orbits which pass near triple-collision we present a special model which is a caricature of the collinear three-body problem. The goal of this paper is to describe the dynamics of this model. The main theorem, that the set of sequences of allowed bounces can be described by a sub-shift of finite type, suggests that a similar result might be possible in the collinear three-body problem.

Rather than three point masses on a line we introduce a fixed bumper between two point masses restricted to a line. This bumper has infinite

378

inertia and zero mass. The presence of the bumper allows for the existence of complicated dynamics and the phase space for this model is qualitatively similar to that of the collinear three-body problem. In this setting we can apply standard dynamical systems techniques and answer some of the questions which remain open in the collinear three-body problem. For the model, we are able to follow the branches of the one-dimensional unstable manifold of triple-collision on the collision manifold in the case of equal masses. We are also able to give a complete list of possible dynamics when the two masses are equal.

We begin with a detailed statement of the model for equal masses and give the equations of motion. We next perform a change of variables to McGehee coordinates and define the collision manifold. We then study the induced flow on the collision manifold. We use our knowledge of the flow on the collision manifold to show how the stable manifold for triple collision sits inside the phase space. With this description, we show what sequences of left and right bounces can occur, our main goal.

2. EQUATIONS OF MOTION

Our model consists of two bodies restricted to a line with positions q_1 and q_2, masses $m_1 = m_2 = 1$ and initial conditions $q_1(0) \leqslant 0 \leqslant q_2(0)$ (see Fig. 1). We denote their momenta by $p_1 = m_1 \dot{q}_1$ and $p_2 = m_2 \dot{q}_2$.

We define a *bumper* to be a fixed massless point so that when either body reaches the bumper, the body bounces elastically. For this paper, the bumper is fixed at the origin. If $q_i = 0$ at time t then we say that the body with position q_i *bounced* at time t, that is, $p_i(t^+) = -p_i(t^-)$. If $q_1 = 0$ at time t then we say that there was a *left bounce* at time t and denote a left bounce with the symbol L. If $q_2 = 0$ at time t then we say that there was a *right bounce* at time t and denote a right bounce with the symbol R. By choosing initial conditions on either side of the bumper, $q_1(0) \leqslant 0 \leqslant q_2(0)$, the position q_1 is always non-positive and the position q_2 is always non-negative.

If at some time t, $q_1(t) = q_2(t) = 0$ we say there is a *triple collision* at time t. We will not continue solutions beyond triple collision (see Theorem 8.1). If a solution begins in triple collision, we say that the solution is an *ejection orbit*, and we denote the collision by the symbol E. A solution which ends
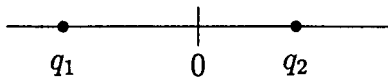

Fig. 1.   Schematic of the collinear one-bumper two-body problem.

in triple collision is a *collision orbit*, and we denote the collision by the symbol C.

When the bodies are away from the bumper, they move under the Hamiltonian system with energy $H = 1/2(p_1^2 + p_2^2) - (q_2 - q_1)^{-1}$. Between bounces solutions are constrained by the two integrals of the two-body problem, total energy, H, and total momentum, $p_1 + p_2$. At a bounce, the momentum of one of the bodies changes sign. (A body cannot hit the bumper with zero momentum.) This resets the total momentum which will be constant until the next bounce. Since the total energy, H, depends on the squares of the momenta, a bounce does not change the total energy. The model system has only one constant of motion, H.

We set the total energy to be negative. This bounds the distance between the two bodies. Since the two bodies cannot escape to infinity and since the bodies are mutually attracting, solutions which are defined for all time must pass through an infinite number of bounces. By keeping track of left and right bounces we can associate a solution to an itinerary of L's and R's. Our goal is to determine what itineraries are realized by solutions of the model.

3. THE GEOMETRY OF THE PHASE SPACE

If we plot the positions the bodies in $\mathbb{R}^2$ as a pair (q_1, q_2), then the configuration space, or set of allowed positions of the bodies, is a subset of the closed second quadrant since $q_1(t) \leqslant 0 \leqslant q_2(t)$. Fixing the total energy to be $h < 0$, the distance between the two bodies is bounded by $-1/h$. This maximum mutual distance can only occur when $p_1 = p_2 = 0$. The line $q_2 - q_1 = -1/h$ acts like the boundary of a Hill's region for our configuration space. The vector field associated with the Hamiltonian, H, is
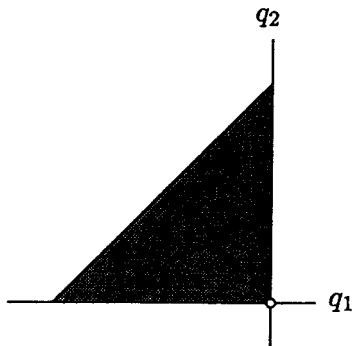

Fig. 2.   Configuration space for negative energy.

undefined at triple collision; thus, the origin must be excluded from our configuration space. The whole configuration space is a filled triangle with vertices $(1/h, 0)$, $(0, -1/h)$, and $(0, 0)$ minus the origin. Positions along $q_1 = 0$ correspond physically with a left bounce, and positions along $q_2 = 0$ correspond physically with a right bounce. The phase space in Hamiltonian coordinates is not compact (Fig. 2).

4. CHANGE OF VARIABLES

To compact our phase space we will use a technique of McGehee's [1] in which the singularity at $q_1 = q_2 = 0$ is replaced by a *collision manifold*. The collision manifold provides a tool for study of how orbits behave as they pass near triple-collision. This transformation is accomplished by a change of variables to polar coordinates and a rescaling of time.

For a point in configuration space, we denote its distance to the origin by the term $r^{2/3}$ and its argument with the positive q_1-axis as θ (see Fig. 3). Notice that θ is bounded by $\pi/2$ and π since we are working in the second quadrant. Associated to the new coordinates r and θ are radial and angular momenta. The coordinates u and v in the following change of variables are related to these momenta.

The change of variables to polar coordinates, (r, θ, u, v) is

$$q_1 = r^{2/3} \cos \theta \qquad\qquad q_2 = r^{2/3} \sin \theta$$
$$p_1 = r^{-1/3}(u \cos \theta - v \sin \theta) \qquad p_2 = r^{-1/3}(u \sin \theta + v \cos \theta).$$
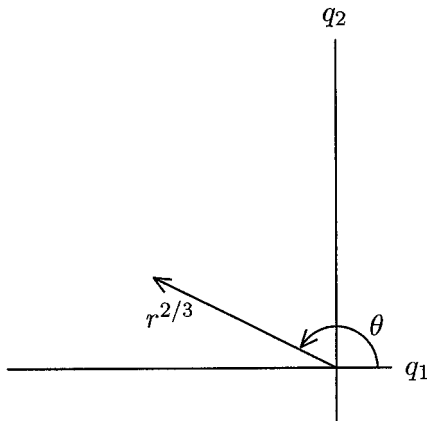

FIG. 3. Change to polar coordinates.

We also let $dt = r\,d\tau$. Then in τ-time or fictitious time, and in the new coordinates, the differential equations becomes

$$\frac{dr}{d\tau} = \frac{3}{2}ru$$

$$\frac{d\theta}{d\tau} = v$$

$$\frac{du}{d\tau} = v^2 + \frac{1}{2}u^2 + V(\theta)$$

$$\frac{dv}{d\tau} = -\frac{1}{2}uv - V'(\theta),$$

where $V(\theta) = (\cos\theta - \sin\theta)^{-1}$ is the angular potential function (see Fig. 4) and V' denotes $dV/d\theta$.

Since r decouples from the system, we may consider the flow in (θ, u, v) coordinates separately. Also, for $r = 0$, $dr/d\tau = 0$ so the set of configurations at triple collision forms an invariant manifold. In these coordinates, the energy equation becomes

$$\tfrac{1}{2}u^2 + \tfrac{1}{2}v^2 + V(\theta) = r^{2/3}h.$$

So for $r = 0$, we have a relationship between θ, u, and v which defines what is called a triple collision manifold. We shall denote this manifold by the symbol M (see Fig. 5).

$$M = \{(\theta, u, v) \mid u^2 + v^2 + 2V(\theta) = 0 \text{ and } \pi/2 \leqslant \theta \leqslant \pi\}.$$

On M, we use the energy relation to write $du/d\tau = 1/2v^2$. This means that the flow on M is non-decreasing in the u direction. Although this flow has no direct physical meaning for the original system (except in the $h = 0$
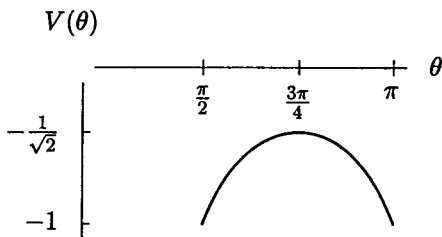
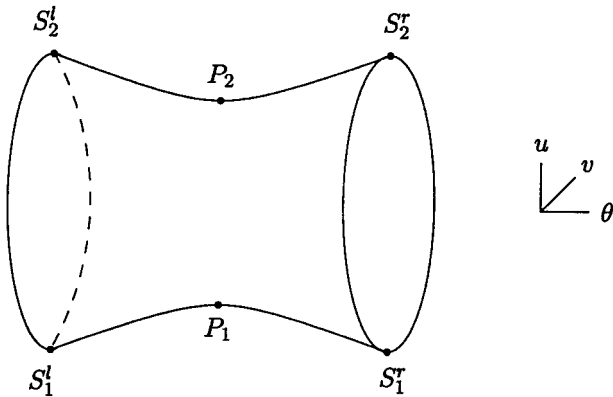

FIG. 4.   Plot of angular potential $V(\theta)$.

FIG. 5.   The collision manifold M and its critical points.

case), real orbits which come close to triple collision must approach the collision manifold and by continuity, must mimic the behavior of the flow on M.

To this point, we have not incorporated the bumper and how it affects the flow. Looking back to the polar change of variables, we see that when $\theta = \pi/2$, q_1 hits the bumper so p_1 changes sign. In polar coordinates, this means $d\theta/dt$ changes sign, so $v = d\theta/d\tau$ changes sign. The analysis at $\theta = \pi$ is the same, at the bumper the v-coordinate changes sign. We may now amend the definition of the collision manifold to include this identification at the bumper.

$$\mathscr{S} = M \left/ \left\{ \begin{matrix} (\pi/2, u, v) \sim (\pi/2, u, -v) \text{ and} \\ (\pi, u, v) \sim (\pi, u, -v) \end{matrix} \right\} \right. .$$

For the rest of the paper we shall picture the collision manifold as M and let solutions jump at its boundary.[1] Solutions on this piece-wise smooth flow are the same qualitatively as on $\mathscr{S}$. We shall not distinguish between M and $\mathscr{S}$ and simply write M for the collision manifold.

5. STUDY OF EQUILIBRIA

To understand the flow for our whole phase space, we must first describe the flow on M. We begin with the equilibria on M.

---

[1] One may ask if there is a third change of variables taking M to a smooth manifold with an associated smooth flow. The answer is yes, namely, $w = -v \sin^{1/3} 2\theta$ $d\tau = \sin^{2/3} 2\theta \, dT$. However, this coordinate system is cumbersome and unrevealing.

THEOREM 5.1.   *The collision manifold, M, has six critical points. In (θ, u, v) coordinates they are*

$$P_1 = (3\pi/4, -\sqrt[4]{2}, 0) \quad P_2 = (3\pi/4, \sqrt[4]{2}, 0)$$
$$S_1^l = (\pi/2, -\sqrt{2}, 0) \quad S_2^l = (\pi/2, \sqrt{2}, 0)$$
$$S_1^r = (\pi, -\sqrt{2}, 0) \quad S_2^r = (\pi, \sqrt{2}, 0)$$

The equilibrium points P_1 and P_2 are saddles. The other four points are not equilibria under the vector field. Because of the identification at the boundaries, solutions beginning at these points can not be continued. The points S_1^l and S_1^r behave like spiral sources, S_2^l and S_2^r behave like spiral sinks on M.

Proof.   From the vector field it is clear that P_1 and P_2 are saddles. For shorthand, we shall denote the vector field by F. For P_1, the matrix $DF|_{P_1}$ has eigenvalues $-2^{1/4}$, $-2^{-3/4}$, and $2^{1/4}$ and associated eigenvectors $(0, 1, 0)$, $(1, 0, 2^{-3/4})$, and $(1, 0, -2^{1/4})$ respectively. Likewise, P_2 is a saddle as the matrix $DF|_{P_2}$ has eigenvalues $2^{1/4}$, $2^{-3/4}$, and $-2^{1/4}$ and associated eigenvectors $(0, -1, 0)$, $(1, 0, 2^{-3/4})$, and $(-1, 0, 2^{1/4})$ respectively.

To prove the claims about $S_{1,2}^{l,r}$, it enough to show that S_1^l acts as a source on M as the rest of the claim follows from the symmetries of the vector field (see Lemma 6.1).

In a deleted neighborhood of S_1^l there are no rest points, so for a solution near S_1^l, $du/d\tau$ is positive except as the solution crosses $v = 0$. Since $v = 0$ is the isocline for $d\theta/d\tau = 0$, the solution crosses $v = 0$ orthogonally. So, in a small deleted neighborhood of S_1^l, solutions move away from S_1^l. It is in this sense that $S_1^{l,r}$ are sinks and $S_2^{l,r}$ are sources. ∎

THEOREM 5.2.   *Solutions in the basin of S_2^r on M pass through an infinite number of bounces.*

Proof.   Let δ be positive and look at a rectangular neighborhood of S_2^r as pictured in Fig. 6. For δ small enough, we can use the energy equation to write u as a function of θ and v so we can project the flow to θ, v coordinates.

For an orbit near S_2^r to terminate after a finite number of circuits, the solution must come in to S_2^r tangent to some angle α measured from the vertical in the θ, v-plane. Since in this δ neighborhood of S_2^r, $dv/d\tau \sim 1 > 0$, it must be that $\alpha \geqslant \pi/2$ else the orbit would come in to S_2^r decreasing in the v coordinate. However for $v < 0$, $d\theta/d\tau < 0$ so the orbit is moving to the left, away from S_2^r, and, as shown above, solutions cross $v = 0$ orthogonally. Since no solution can terminate at S_2^r by coming in tangent, every solution crosses $\theta = \pi$ an unbounded number of times as τ increases. ∎
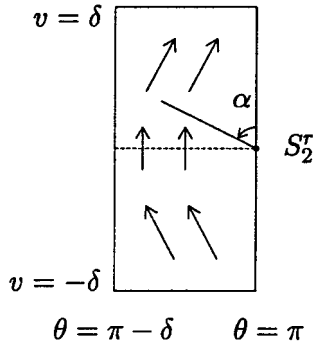
FIG. 6.   Rectangular neighborhood of S_2^r.

6. SYMMETRY OF SOLUTIONS

The equations of motion in McGehee coordinates, hence the flow, have two symmetries: a mirror symmetry and a time symmetry, reversibility. The symmetries are easy to verify. Reversibility is standard in Hamiltonian systems and the mirror symmetry is present because we are considering the special case of equal masses. Since the two bodies have the same mass we can switch their roles yielding the mirror symmetry. These symmetries apply to any solution, not just ones on M.

LEMMA 6.1.   *There are two symmetries to the flow*:

Mirror Symmetry	*Reversibility*
$\bar{\theta} = \dfrac{3\pi}{2} - \theta$	$\bar{u} = -u$
$\bar{v} = -v$	$\bar{v} = -v$
	$\bar{\tau} = -\tau$

If (θ, u, v) is a solution in time τ   *If (θ, u, v) is a solution in time τ*

then so is $(\bar{\theta}, u, \bar{v})$ in τ   *then so is $(\theta, \bar{u}, \bar{v})$ in $\bar{\tau}$.*

Proof.   The calculations are straightforward and left to the reader.   ∎

7. THE FLOW ON THE COLLISION MANIFOLD

A solution passing through several bounces has an associated *itinerary* of L's and R's. If a solution is on the stable manifold for P_1 then we end its itinerary with the symbol C. If a solution is on the unstable manifold for P_2 then we begin its itinerary with the symbol E. On M, however, P_1 and P_2 each have a stable and unstable manifold. To distinguish the unstable manifold of P_1 and P_2 on M we begin the itinerary with the symbol P_1 or P_2. To distinguish the stable manifold of P_1 and P_2 on M we end the itinerary with the symbol P_1 or P_2. We next determine the itinerary of one branch of the one-dimensional unstable manifold of P_1. This will be enough information to determine the itinerary of all the branches of stable and unstable manifolds at P_1 and P_2 on M.

THEOREM 7.1. *One branch of the unstable manifold of* P_1 *follows the itinerary* $P_1 LRLRRR...$, *the other branch follows the itinerary* $P_1 RLRLLL...$.

Proof (outline of proof).   We can find the location of the first intersection of the unstable manifold with the plane $\theta = \pi/2$ analytically. The surface corresponding to zero momentum given by the relation $p_1 + p_2 = 0$, or in McGehee coordinates, $u(\cos\theta + \sin\theta) + v(\cos\theta - \sin\theta) = 0$ is invariant under the flow. The intersection of the zero momentum manifold and M are solutions. One of the arcs of intersection passes through P_1 and since the vector field points away from P_1 along this arc, this is the unstable manifold of P_1. It is easy to check that the first intersection of the unstable manifold with the plane $\theta = \pi/2$ is at $u = v = -1$. That is $P_1 L$ has a u-coordinate of -1.

One can use technical estimates (see Lemma 7.2) to continue following the branches of the unstable manifold of P_1 and show that the solution continues across M and intersects the plane at $\theta = \pi$ with a negative u-coordinate. That is the points $P_1 LR$ and $P_1 RL$ each have a negative u-coordinate. By symmetry (see Lemma 6.1) the stable manifold for P_2 pulls back two bounces to be just above the unstable manifold for P_1. That is, the points on M with the itinerary RLP_2 and LRP_2 are just above $u = 0$. This says that the solution for the unstable manifold bounces at least twice more. With a second technical estimate (see Lemma 7.3) we can verify that the solution is then caught in the basin for $S_2^{l,r}$. See Figs. 7 and 9.   ∎

LEMMA 7.2.   *The points* $P_1 LR$, *and* $P_1 RL$ *each have a negative u-coordinate.*

Proof.   Recall that on M, $du/d\tau = v^2/2$ and $d\theta/d\tau = v$. From this we see that $du/d\theta = v/2$. For the initial condition, $P_1 R$, that is at $\tau = 0$, $\theta = \pi$,
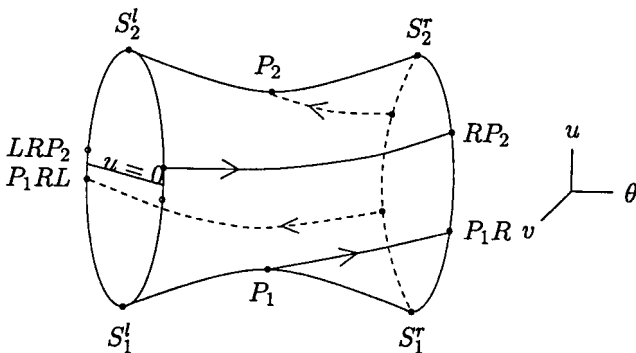
FIG. 7. The first two bounces on one unstable branch of P_1 and its time-symmetric stable manifold of P_2.

$u = -1$, $v = -1$, we can rewrite v as $-\sqrt{-u^2 - 2V(\theta)}$. We now want to bound the derivative, $du/d\theta$.

For $\pi/2 \leqslant \theta \leqslant \pi$ we have

$$-1 \leqslant V(\theta) \leqslant -\frac{1}{\sqrt{2}}$$

$$\sqrt{2} \leqslant -2V(\theta) \leqslant 2$$

$$-\frac{1}{2}\sqrt{2 - u^2} \leqslant \frac{du}{d\theta} \leqslant -\frac{1}{2}\sqrt{\sqrt{2} - u^2}.$$

Since the solution stays below P_2 whose u-coordinate is $\sqrt[4]{2}$, the function $u(\theta)$, is strictly decreasing hence invertible so $\theta(u)$ is well-defined and

$$-\frac{2}{\sqrt{\sqrt{2} - u^2}} \leqslant \frac{d\theta}{du} \leqslant -\frac{2}{\sqrt{2 - u^2}}.$$

We integrate these three terms to see if the change in θ is greater than $-\pi/2$. If so, then θ crossed $\pi/2$ before u reached zero. We also make the inequalities strict since neither bound on $d\theta/du$ maintains equality for the entire path between $P_1 L$ and $P_1 LR$.

$$-\int_{u=-1}^{0} \frac{2}{\sqrt{\sqrt{2} - u^2}} \, du < \int_{u=-1}^{0} \frac{d\theta}{du} \, du < -\int_{u=-1}^{0} \frac{2}{\sqrt{2 - u^2}} \, du$$

$$-2 \arcsin(2^{-1/4}) < \theta(0) - \theta(-1) < -2 \arcsin(2^{-1/2})$$

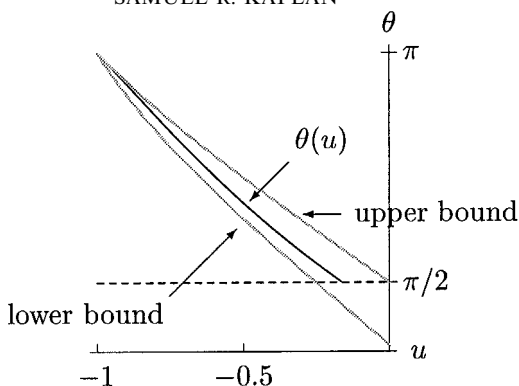$$\pi - 2 \arcsin(2^{-1/4}) < \theta(0) < \frac{\pi}{2}.$$

FIG. 8.   Plot upper and lower bounds for $\theta(u)$ for the path between $P_1 L$ and $P_1 LR$.

Since $\theta(0) < \pi/2$, the curve $\theta(u)$ crossed $\pi/2$ for $u < 0$ hence the u-coordinate of $P_1 LR$ is negative.   ∎

LEMMA 7.3.   *The point $P_1 LRLR$ is in the basin of S_2^r.*

Proof.   We know that the u-coordinate of $P_1 RL$ is negative, but we need a lower bound for it as well. From Lemma 7.2 we have the inequality

$$-\frac{2}{\sqrt{\sqrt{2} - u^2}} \leqslant \frac{d\theta}{du}.$$

A lower bound for the u-coordinate of $P_1 RL$ is the value for which the curve, which bounds the path from $P_1 R$ to $P_1 RL$ from below, crosses $\theta = \pi/2$ (see Fig. 8). That is, we want to solve for u_x such that

$$-\int_{u=-1}^{u_x} \frac{2}{\sqrt{\sqrt{2} - u^2}} \, du = -\pi/2$$

$$2 \arcsin(2^{-1/4}) + 2 \arcsin(u_x 2^{-1/4}) = \frac{\pi}{2}.$$

Since $u_x < 0$ we know that $\arcsin(u_x) < u_x$.

$$2u_x 2^{-1/4} > 2 \arcsin(u_x 2^{-1/4}) = \frac{\pi}{2} - 2 \arcsin(2^{-1/4})$$

$$u_x > 2^{-3/4} \left(\frac{\pi}{2} - 2 \arcsin(2^{-1/4}) \right)$$

$$> -0.26.$$

Since the u-coordinate of $P_1 RL$ is negative, the u-coordinate of LRP_2 is positive. Since $P_1 RL$ is below LRP_2, it must cross to the right, so $P_1 RLR$ exists. We next want to show that the u-coordinate of $P_1 RLR$ is larger than the absolute value of the u-coordinate of $P_1 RL$. It is enough to show that the u-coordinate of $P_1 RLR$ is larger than 0.26.

To do this, we calculate the value of u_y so that

$$\int_{-u_y}^{u_y} \frac{2}{\sqrt{\sqrt{2} - u^2}} \, du = \frac{\pi}{2}.$$

The solution to this equation is the boundary between initial conditions whose sum of initial and final u-coordinates is positive and those whose sum is negative. Notice that we are now assuming that we are crossing from left to right, that is $v > 0$.

$$\int_{-u_y}^{u_y} \frac{2}{\sqrt{\sqrt{2} - u^2}} \, du = \frac{\pi}{2}$$

$$4 \arcsin(u_y 2^{-1/4}) = \frac{\pi}{2}$$

$$u_y 2^{-1/4} = \sin(\pi/8)$$

$$u_y = \sqrt{(\sqrt{2})/2} \approx 0.455.$$

Since the u-coordinate of $P_1 RL > -0.26 > -u_y$ we have that the u-coordinate of $P_1 RLR > u_y > 0.26$, that is, the u-coordinate of $P_1 RLR > u$-coordinate of RLP_2. The u-coordinate of $P_1 RLR$ is less that the u-coordinate of RP_2 since the inequality held for their pre-images under the return map. Since $P_1 RLR$ is between RP_2 and RLP_2, it must cross to the right. Since $P_1 RLRL$ is above LP_2, it is trapped in the basin of S_2' (Fig. 9). ∎
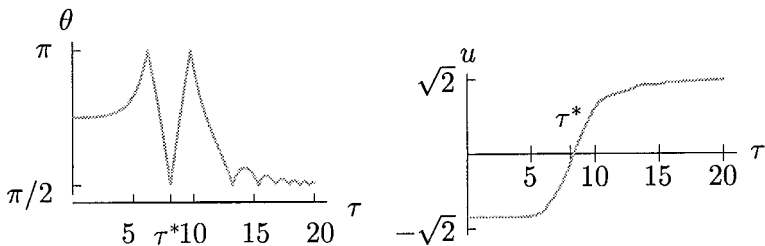

FIG. 9.   The time-τ plots of the θ and u coordinates of the unstable branch of P_1 shown in Fig. 7. At time $\tau = \tau^*$, the solution passes through the right face for the first time. Note that $-0.26 < u(\tau^*) < 0$.

8. BLOCK REGULARIZATION

One calls a triple-collision (block) regularizable if solutions can be extended past triple-collision with continuity with respect to initial conditions (see [McG]). As in the collinear three-body problem, triple-collision is not regularizable for this model.

THEOREM 8.1.   *Triple collision is not block regularizable.*

Proof.   The equilibrium, P_1 has a two-dimensional stable manifold and a one dimensional unstable manifold. The unstable manifold lies entirely on M.

Pick a small disk of initial conditions centered about the invariant line, $\theta = 3\pi/4$, $v = 0$ parallel to the $u - v$ plane with a u-coordinate close to that of P_1. Following this disk of initial conditions forms a tubular neighborhood of solutions which lead to and near triple collision at P_1. This tube splits up and part of that neighborhood follows one arm up to S_2^l and part follows up the other arm to S_2^r (see Theorem 7.1).

So near an orbit leading to triple collision is an orbit which has q_1 bouncing at the bumper several times consecutively while q_2 moves off or vice versa. So there is no way to continue triple collision preserving continuity with respect to initial conditions This is the same reason that triple-collision is not regularizable in the collinear three-body problem.   ∎

9. PROPERTIES OF THE FULL FLOW

We will denote the phase space for the model as $\mathcal{M}$.

$$\mathcal{M} = \{(\theta, u, v) \mid u^2 + v^2 + 2V(\theta) \leqslant 0 \text{ and } \pi/2 \leqslant \theta \leqslant \pi\}.$$

The phase space is bounded by M and a disk in the plane $\theta = \pi/2$ of radius $\sqrt{2}$ centered at $u = v = 0$ corresponding to a left bounce and second disk in the plane $\theta = \pi$ of radius $\sqrt{2}$ centered at $u = v = 0$ corresponding to a right bounce. Orbits in the phase space continue past bounces the same way as on M, namely by changing the sign of the v coordinate at the time of the bounce.

Comparison to Hamiltonian Coordinates

To assist the reader's understanding of the new coordinates, we compare it to the Hamiltonian coordinate system. The origin, a singularity in Hamiltonian coordinates, has been blown up to be all of M. The boundary

of Hill's region $(q_1 + q_2 = -1/h)$ has become the θ-axis (where r is at a maximum).

What had been the q_1-axis now corresponds to the intersection of the new phase space and the $\theta = \pi$ plane. This intersection we call the *right face* of the phase space. Likewise, the q_2-axis corresponds to the intersection of the new phase space and the $\theta = \pi/2$ plane. This intersection we call the *left face*. See Fig. 10.

Left bounces occur on the left face. Right bounces occur on the right face. For an orbit to be near triple collision in configuration space means the orbit is near M in McGehee coordinates.

Ejection-Collision Orbit

There is a connecting orbit between P_1 and P_2 in the interior of M. For $\theta = 3\pi/4$ and $v = 0$, both $d\theta/d\tau$ and $dv/d\tau$ vanish. Thus the u-direction between P_2 and P_1 forms a one-dimensional invariant manifold, EC, with the differential equation $du/d\tau = (u^2 - \sqrt{2})/2$.
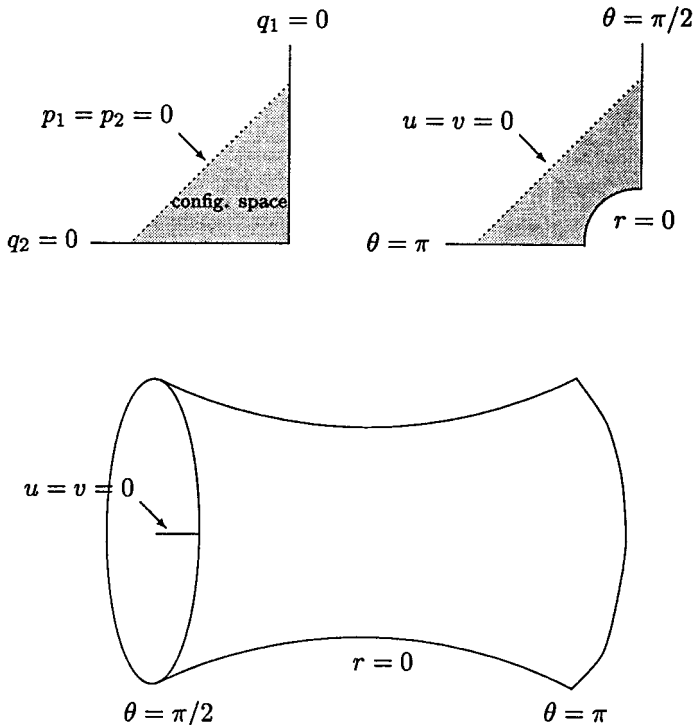
FIG. 10. The two top figures are the configuration space in rectangular and polar coordinates. The bottom picture is of M and the θ-axis in $\mathcal{M}$.

The solution of this differential equation on the set where $\theta = \pi/4$ and $v = 0$ is

$$u(\tau) = \sqrt[4]{2} \tanh (K - \tau/\sqrt[4]{8}),$$

where K is a constant of integration determined by the initial condition. This function is strictly decreasing from P_2 to P_1. Thus solutions with initial conditions on this line are defined for all time and have an α-limit set at P_2 and an ω-limit set at P_1. The radial coordinate along this solution is increasing for $u > 0$ and decreasing for $u < 0$ and zero at P_1 and P_2. Since the θ-coordinate is invariant, there are no bounces. Thus a solution along this line in backwards time comes from ejection and in forwards time goes to collision. These solutions are called the *ejection-collision* orbits.

For an orbit in the interior of M to begin in collision or end in collision (respectively ejection or collision), is must limit onto P_1 in forward time or limit onto P_2 in backward time. This is equivalent to saying that ejection orbits are in the unstable manifold of P_2 and that collision orbits are in the stable manifold of P_1. These manifolds are the key to understanding the dynamics of the flow and are related by the symmetries of the differential equations in McGehee Coordinates.

Physical Interpretation of the Line $v = 0$ on the Faces

On each face the line $v = 0$ is fixed by the identity corresponding to a bounce. Initial conditions on these lines corresponds to setting one body at the bumper with zero momentum. This body can not leave the bumper so the set of such conditions is invariant under the flow. The other body moves along the solution to a central force problem since it is attracted to the body trapped at the bumper. So initial conditions on the line $v = 0$ at either face can be easily solved. Moreover, initial conditions not on the line $v = 0$ on either face can not limit onto the line $v = 0$ at either face except at the fixed points S_1^l, S_1^r, S_2^l, S_2^r. For the remainder of this paper, we shall treat the line $v = 0$ on either face as a line of fixed points.

10. ASSIGNING SYMBOL SEQUENCES

In order to understand the dynamics of the phase space we want to assign a symbol sequence to every solution of the equations of motion. We shall assign an itinerary of bounces for each solution in the full phase space just as we did when we were restricted to M. Every time a solution passes through a left bounce, or equivalently, the left face, we shall append the sequence of bounces by an L. Likewise, every time a solution passes through a right bounce, or equivalently, the right face, we shall append the

sequence of bounces by an R. If a solution ends in triple collision, we shall end the sequence by C. If a solution begins in triple collision, we shall begin its sequence with an E (for ejection).

In this way, we can map any solution in the phase space to a symbol sequence space. Thus the symbol sequence space is the union of biinfinite sequences of L's and R's, left-infinite sequences of L's and R's ending in C, right-infinite sequences of L's and R's beginning with E and finite sequences of L's and R's beginning with E and ending with C. Any solution on the ejection-collision orbit maps to the sequence EC, for example.

We can use the symmetries in the previous section to say how the itinerary of an initial condition changes if we apply a symmetry to that initial condition. Let $\bar{L} = R$, $\bar{R} = L$, $\bar{E} = E$ and $\bar{C} = C$. Then the time symmetry transforms the itinerary $(a_1 a_2 a_3 \cdots a_n)$ to $(a_n a_{n-1} \cdots a_1)$ and back again. If $a_1 = E$ then the time symmetry transforms the itinerary $(E a_2 a_3 \cdots a_n)$ to $(a_n \cdots a_3 a_2 C)$ and back again. The mirror symmetry transforms the itinerary $(a_1 a_2 a_3 \cdots a_n)$ to $(\bar{a}_1 \bar{a}_2 \bar{a}_3 \cdots \bar{a}_n)$. The main problem of describing the dynamics of the collinear one-bumper two-body problem is asking if the map from solution to symbol sequences is onto and if it is not onto, what sequences are missed and why. To do this we must next set-up a return map on an appropriately chosen Poincaré slice.

11. CHOICE OF POINCARÉ SLICE

In order to choose a Poincaré slice we must find a manifold of codimension-one which is transverse to the flow and through which all or almost all orbits pass. The following lemmas make the location of bounces, that is the left and right faces of the phase space, a natural choice for our Poincaré slice.

Recall that bounces occur when θ equals $\pi/2$ or π, that is, at the left and right faces of M. Because of the identification at a bounce, we only need to consider half of each face. We join the half of the left face (at $\theta = \pi/2$, $v < 0$) to half of the right face (at $\theta = \pi$, $v > 0$) to form our Poincaré slice, Σ. We define the Poincaré map on Σ to be the first return to Σ under the flow. We will denote the Poincaré map by the symbol $\wp$.

LEMMA 11.1. *All solutions which pass though the left or right face do so transversely.*

Proof.   It is enough to show that solutions which reach the left or right face have a tangent vector with a non-zero θ-component since the left and right faces are perpendicular to the θ-axis. Since $d\theta/d\tau = v$, the tangent vector has a non-zero θ-component except at $v = 0$. However such points

are fixed by the identification at the bounces. No solution can land on this line since that would mean a mass could hit the bumper with zero momentum. ∎

LEMMA 11.2. *Except for solutions whose initial conditions are along the line $\theta = 3\pi/4$, $v = 0$ or on the critical points of the vector field on M, all solutions pass through at least one bounce.*

Proof. In the classic two-body problem, for negative energy, any initial condition leads to double collision in finite time. In our model, the bumper interferes with the path towards collision unless the two bodies collide at the origin, i.e., a triple collision orbit. If we follow triple-collision orbits in backwards time, all of them will tend towards double collision. The bumper will interfere unless the two bodies ejected from the origin, i.e., an ejection orbit. The ejection-collision orbit in the two-body problem where ejection and collision both occur at the origin must be symmetric about the origin, that is, along such a solution, $\theta = 3\pi/4$. The only invariant set with this condition is the ejection-collision orbit we identified in Section 1. Except this ejection-collision orbit, then, all solutions in the interior of $\mathscr{M}$ pass through at least one bounce.

The same argument applies to the case of zero energy, hence all solutions on M pass through at least on bounce except the critical points of the vector field on M. ∎

12. THE STABLE MANIFOLD FOR TRIPLE COLLISION

We want to understand how the two-dimensional stable manifold for triple-collision, $W^s(P_1)$, intersects Σ. This is the key to unlocking the dynamics because if two points on Σ have different itineraries under the flow, then along any path on Σ connecting these points, there is at least one initial condition which cannot decide which itinerary to follow and thus leads to triple collision. The pieces of $W^s(P_1)$ break up Σ into regions with common itineraries. If we can understand how $W^s(P_1)$ intersects Σ, we then have a way to describe allowed sequences of left and right bounces without further bounces in between.

As stated in the previous section, we can label each piece of stable manifold by the itinerary of that piece. For example, the sequence RC means all those points which begin at a right bounce and end in triple collision.

The curves LC and RC cut Σ into four regions. In the interior of these regions we know the first two symbols of the itinerary of each initial condition. The regions can be labeled LR, LL, RR, and RL. If we continue
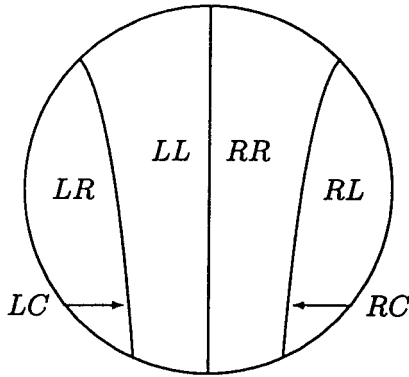
FIG. 11.   The first pullback of the stable manifold for triple collision divides Σ into four regions.

to pull back the stable manifold of triple-collision we can continue labeling regions with the appropriate dynamics.

With respect to further pullbacks, though, LC and RC are as far as exact solutions can take us. To continue pulling back the stable manifold for triple collision we must rely on the geometry of the flow (for proofs) or numerics (for pictures).

Reversibility says that if we take LC and flip it about $u = 0$ we get EL. Since we are pulling pieces of stable manifold backwards in time, it is exactly EL and ER which determine which points on LC and RC pull back to the left and which to the right (Fig. 11).

For free we get that the stable manifold for collision and the unstable manifold for ejection intersect transversely (see Fig. 12).
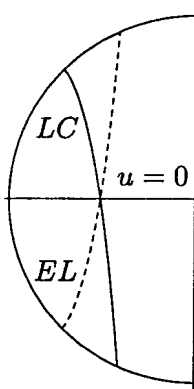
FIG. 12.   Transverse intersection of LC (solid) and EL (dashed).

LEMMA 12.1. *We can solve for the implicit equations for RC and LC on Σ. In u, v coordinates, for LC we have the relation*:

$$\sigma(u - v)((2\sigma + 1)\,\pi + sAB + 2\Omega) + A^3 = 0,$$

where $\Omega = \arctan(sA^{-1}(B - 2B^{-1}))$, $A = \sqrt{4 - B^2}$, $B = u + v$, $s = \operatorname{sign}(B)$ and $\sigma = 1 + s - s^2$. The equation for RC is obtained by reflecting LC over the u-axis.

Proof.   The proof is a lengthy series of unrevealing calculations.

Since there are no bounces in the course of orbits whose initial conditions are on *LC*, the orbit is entirely a collinear two-body problem. We proceed to calculate *LC* in three steps:

1.   In a mutual distance coordinate $\rho = q_2 - q_1$, we solve the original Hamiltonian system for time as a function of ρ, $t(\rho)$.

2.   We find the time to collision, $t^* = t(0)$ as a function of the initial conditions.

3.   An initial condition on the left half of Σ is on *LC* if the collision occurs at $q_1 = q_2 = 0$. Since the center of mass moves linearly, we set $\alpha t^* + \beta = 0$ where $\alpha = (p_1(0) + p_2(0))/2$ and $\beta = (q_1(0) + q_2(0))/2$. It is now only a matter of changing variables to u and v to see that the relation $\alpha t^* + \beta = 0$ becomes the relation stated in this Lemma.

Step 1.   Let $\rho = q_2 - q_1$ be the mutual distance and $\rho_c = (q_2 + q_1)/2$ denote the center of mass. Then

$$\ddot{\rho} = \ddot{q}_2 - \ddot{q}_1 = \dot{p}_2 - \dot{p}_1 = -\frac{2}{(q_2 - q_1)^2} = -2\rho^{-2}$$

so we have a second-order differential equation for ρ. Taking the second derivative of ρ_c we have

$$\ddot{\rho}_c = \tfrac{1}{2}(\ddot{q}_1 + \ddot{q}_2) = \tfrac{1}{2}(\dot{p}_1 + \dot{p}_2) = 0.$$

That is ρ_c is linear in real time t,

$$\rho_c(t) = \dot{\rho}_c(0)\,t + \rho_c(0).$$

For the moment we are assuming there is no bumper. Suppose that the two bodies collide at time t^*. This binary collision corresponds to a triple collision in the collinear one-bumper two-body problem if the collision takes place at the bumper, that is if

$$\alpha t^* + \beta = 0,$$

where $\alpha = \dot{p}_c(0) = (p_1(0) + p_2(0))/2$ and $\beta = p_c(0) = (q_1(0) + q_2(0))/2$. We want to find all the initial conditions on the left face so that the relation $\alpha t^* + \beta = 0$ holds.

First we must compute t^* for initial conditions on the left face. We begin with the second-order differential equation for ρ,

$$\ddot{\rho} = -2\rho^{-2}$$

$$\int_{s=0}^{t} \dot{\rho}\ddot{\rho}\, ds = \int_{s=0}^{t} -2\rho^{-2}\dot{\rho}\, ds$$

$$\frac{1}{2}\dot{\rho}^2 = \frac{2}{\rho} + k$$

$$\frac{1}{2}\dot{\rho}^2 - \frac{2}{\rho} = k.$$

This last equation is the energy equation in the center of mass reference frame. The energy, k, is determined by the initial conditions, $\dot{\rho}(0)$ and $\rho(0)$.

The energy relation yields two first-order autonomous differential equations,

$$\dot{\rho} = \pm\sqrt{2(k + 2\rho^{-1})}$$

Separating and integrating we have,

$$\pm \int_{s=0}^{t} \frac{\dot{\rho}}{\sqrt{2(k + 2\rho^{-1})}}\, ds = \int_{s=0}^{t} ds$$

$$\pm \frac{1}{\sqrt{2}\,k}\left(\rho R + \frac{1}{\sqrt{-k}} \arctan\left(\frac{1 + k\rho}{\sqrt{-k}\,\rho R}\right)\right) = t + C,$$

where $R = \sqrt{2 + 2\rho^{-1}}$. Solving for $t_{\pm}(\rho)$ we have

$$t_{\pm}(\rho) = C_{\pm} \pm \frac{1}{\sqrt{2}\,k}\left(\rho R + \frac{1}{\sqrt{-k}} \arctan\left(\frac{1 + k\rho}{\sqrt{-k}\,\rho R}\right)\right),$$

where $C_{\pm}$ are constants of integration.

Now we need to study these two functions of mutual distance, ρ. First we take the limit of $t_{\pm}(\rho)$ as ρ approaches zero since this will determine the values of $C_{\pm}$.

Since

$$\lim_{\rho \to 0} \rho R = \lim_{\rho \to 0} \sqrt{\rho(k\rho + 2)} = 0$$

we have

$$\lim_{\rho \to 0} \arctan\left(\frac{1+k\rho}{\sqrt{-k}\,\rho R}\right) = \lim_{x \to \infty} \arctan(x) = \frac{\pi}{2}.$$

With these limits in hand we can evaluate the limit of $t_{\pm}(\rho)$ as ρ goes to zero:

$$\lim_{\rho \to 0} t_{\pm}(\rho) = C_{\pm} \mp \pi(-2k)^{-3/2}$$

The branch, $t_+(\rho)$, corresponds to an initial condition of $\dot{\rho}(0) > 0$, that is the two bodies are heading away from each other. This means for small ρ, $dt_+/d\rho$ should be positive. Since we want $t_+(0) = 0$ we have $C_+ = \pi(-2k)^{-3/2}$.

To find C_- we must determine the maximum ρ as a function of k and evaluate $t_+(\rho_{\max})$ and set $t_-(\rho_{\max}) = t_+(\rho_{\max})$. We do this because we want the branches to meet so that we can pass from one to the other continuously. We will soon see that $\dot{\rho} = 0$ when ρ is at its maximum, hence it is the condition for the point which connects the branches of t_- and t_+.

Calculating $dt_+/d\rho$ we have

$$\frac{dt_+}{d\rho} = 1 \bigg/ \left|\frac{d\rho}{dt}\right| = \frac{1}{\sqrt{2(k+2\rho^{-1})}},$$

which has a singularity when $\rho = -2/k$, that is $\rho_{\max} = -2/k$. Now we evaluate $t_+(-2/k)$.

Since

$$\lim_{\rho \to -2/k} \rho R = \lim_{\rho \to -2/k} \sqrt{\rho(k\rho + 2)} = 0$$

we have

$$\lim_{\rho \to -2/k} \arctan\left(\frac{1+k\rho}{\sqrt{-k}\,\rho R}\right) = \lim_{x \to -\infty} \arctan(x) = -\frac{\pi}{2}.$$

We can calculate the limit of $t_+(\rho)$ as ρ increases to $\rho_{\max}$:

$$\lim_{\rho \to \rho_{\max}} t_+(\rho) = 2\pi(-2k)^{-3/2}.$$

Setting $t_+(\rho_{\max}) = t_-(\rho_{\max})$ we have that $C_- = 3\pi(-2)^{3/2}$. We have solved for $t_{\pm}(\rho)$, time as a function of mutual distance for the solution.

Step 2. What we would like is the function which tells us time to collision given an initial condition. Since the time elapsed from ejection to collision is $4\pi(-2k)^{-3/2}$ the function which gives us time to collision, $t_{\pm}^{*}(\rho) = 4\pi(-2k)^{-3/2} - t_{\pm}(\rho)$.

We now drop the subscript $\pm$ and write $t*(\rho)$ as a branched function.

$$
t^{*}(\rho) = \begin{cases} 3\pi(-2k)^{-3/2} - \dfrac{1}{\sqrt{2}\,k}\left(\rho R + \dfrac{\omega}{\sqrt{-k}}\right) & \text{if } \dot{\rho}(0) \geqslant 0 \\[3mm] \pi(-2k)^{-3/2} + \dfrac{1}{\sqrt{2}\,k}\left(\rho R + \dfrac{\omega}{\sqrt{-k}}\right) & \text{if } \dot{\rho}(0) \leqslant 0, \end{cases}
$$

where

$$
\omega = \arctan\left(\frac{1+k\rho}{\sqrt{-k}\,\rho R}\right).
$$

We define $\sigma = -1$ when $(\dot{\rho}(0))$ is negative and $\sigma = 1$ otherwise. Then for $s = $ sign of $\dot{\rho}$, $\sigma = 1 + s - s^2$. Using σ, we can rewrite $t^{*}(\rho)$ as

$$
t^{*}(\rho) = (2+\sigma)\,\pi(-2k)^{-3/2} - \frac{\sigma}{\sqrt{2}\,k}\,\rho R + 2\sigma(-2k)^{-3/2}\,\omega
$$

$$
= \sigma(-2k)^{-3/2}((2\sigma+1)\,\pi + 2\sqrt{-k}\,\rho R + 2\omega).
$$

Now we must change variables to (θ, u, v) coordinates and find the time to collision for initial conditions on the left face, that is, initial conditions of the form $\theta(0) = \pi/2$, $v(0) > 0$ and $u(0)^2 + v(0)^2 < 2$.

Recall the change of variables from Hamiltonian coordinates to McGehee coordinates.

$$
q_1 = r^{2/3}\cos\theta \qquad p_1 = r^{-1/3}(u\cos\theta - v\sin\theta)
$$

$$
q_2 = r^{2/3}\sin\theta \qquad p_2 = r^{-1/3}(u\sin\theta + v\cos\theta).
$$

When $\theta = \pi/2$ the change of variables becomes

$$
q_1 = 0 \qquad p_1 = -r^{-1/3}v
$$

$$
q_2 = r^{2/3} \qquad p_2 = -r^{-1/3}u.
$$

We will use the energy relation to eliminate r in a moment. For now we retain r to keep the algebra simple. In addition, we define the terms $A = \sqrt{4 - B^2}$, $B = u + v$, and $s = \text{sign}(B)$.

$$\rho = q_2 - q_1 = r^{2/3}$$

$$\dot{\rho} = p_2 - p_1 = r^{-1/3}(u + v) = r^{-1/3}B$$

$$k = \frac{1}{2}\dot{\rho}^2 - \frac{2}{\rho} = \frac{1}{2}r^{-2/3}(u + v + 2)(u + v - 2) = -\frac{1}{2}r^{-2/3}A^2$$

$$R = \sqrt{k + 2\rho^{-1}} = \sqrt{\frac{(u+v)^2}{2r^{2/3}}} = \frac{|u+v|}{\sqrt{2}\,r^{1/3}} = \frac{sB}{\sqrt{2}\,r^{1/3}}$$

Simplifying terms which appear in the expression for $t^*(\rho)$ we have,

$$2\sqrt{-k}\,\rho R = 2\left(\frac{1}{\sqrt{2}}\frac{A}{r^{1/3}}\right)(r^{2/3})\left(\frac{sB}{\sqrt{2}\,r^{1/3}}\right) = sAB$$

$$2(1 + k\rho) = 2\left(1 - \frac{1}{2}\left(\frac{A}{r^{1/3}}\right)^2 r^{2/3}\right) = 2 - A^2 = B^2 - 2$$

Therefore, we can rewrite t^* as

$$t^*(\rho) = \sigma(-2k)^{-3/2}\left((2\sigma + 1)\,\pi + sAB + 2\Omega\right),$$

where $\Omega = \arctan(sA^{-1}(B - 2B^{-1}))$ (Figs. 13 and 14).

Step 3. We now return to simplifying terms in the relation $\alpha t^* + \beta = 0$.

$$\dot{\rho}_c(0) = \frac{1}{2}(p_1(0) + p_2(0)) = \frac{1}{2}(u - v)\,r^{-1/3}$$

$$\rho_c(0) = \frac{1}{2}(q_1(0) + q_2(0)) = \frac{1}{2}r^{2/3}$$

$$(-2k)^{-2/3} = \left(\frac{r^{2/3}}{A^2}\right)^{3/2} = \frac{r}{A^3}.$$

Finally we can simplify the left-hand side of the needed relation, since

$$\alpha t^* + \beta = \tfrac{1}{2}(p_1(0) + p_2(0))\,t^* + \tfrac{1}{2}(q_1(0) + q_2(0))$$

and we need $\alpha t^* + \beta = 0$ for triple collision, we have

$$0 = \tfrac{1}{2}(u - v)\,r^{-1/3}t^* + \tfrac{1}{2}r^{2/3}.$$
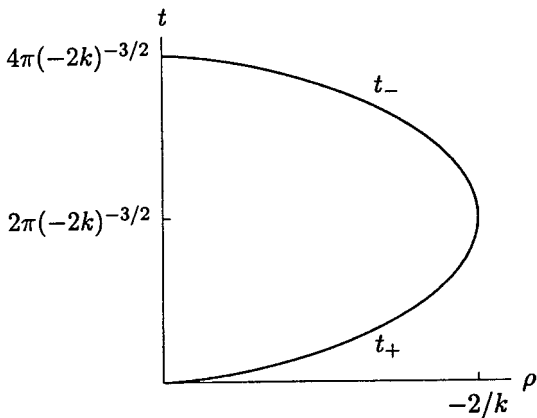
FIG. 13.   Plot of the two branches of $t(\rho)$.

Simplifying yields

$$0 = (u - v)\, t^* + r$$
$$0 = (u - v)\, \sigma(-2k)^{-3/2}\left((2\sigma + 1)\,\pi + sAB + 2\Omega\right) + r$$
$$0 = (u - v)\, \sigma r A^{-3}\left((2\sigma + 1)\,\pi + sAB + 2\Omega\right) + r$$
$$0 = \sigma(u - v)\left((2\sigma + 1)\,\pi + sAB + 2\Omega\right) + A^3. \quad \blacksquare$$
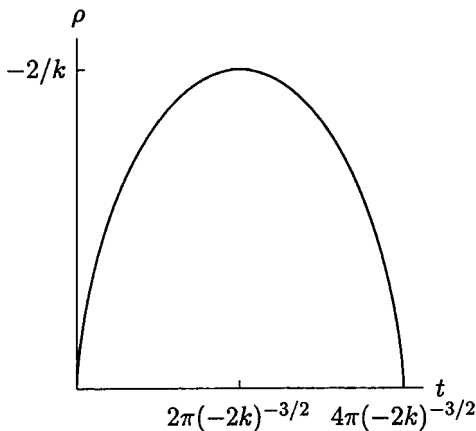
FIG. 14.   Solution of ρ as a function of time, t.

13. SYMBOLIC DYNAMICS OF SOLUTIONS

A piece of stable manifold for triple collision will split under one pullback of $\wp$ if it intersects either *EL* or *ER*. The point of intersection has no pre-image under $\wp$ and serves as a divider between points with a pre-image on the left face and nearby points with a pre-image on the right face. Conversely, if a piece of stable manifold for triple collision does not intersect either *EL* or *ER* then it will not split under one pullback of $\wp$.

The curves *ER* and *RC* intersect at one point along $u = 0$. This means that the top part of *RC* will switch sides and pull back to *LRC*, while the bottom part of *RC* will pull back to the same side and be denoted *RRC*. Each of these new curves will have two end points on the boundary of Σ. The initial conditions on *RC* near to but above $u = 0$ will just miss triple collision, move up the ejection-collision orbit and out along the stable manifold of P_2 to make the top point of *LRC*. All of *LRC* is above $u = 0$ which we can show by studying the flow on M (see Theorem 13.2). The initial conditions on *RC* just below $u = 0$ likewise become the top point of *RRC*. The bottom point of *RRC* is below the bottom point of *RC*. The top points of the second pullbacks are easy to solve for directly and have coordinates $(-1, 1)$ and $(1, 1)$ respectively on Σ. By mirror symmetry, we know the positions of *RLC* and *LLC*.

We would like to continue pulling back pieces of stable manifold and to verify if they intersect *EL* and if so how often. To verify these intersections, we need a technical lemma.

LEMMA 13.1. *Let a be the v coordinate of the intersection of $u = 0$ and LC on Σ. Let $\phi \colon [-\sqrt{2}, a) \to \mathbb{R}$ so that $x \mapsto$ the v coordinate of $\wp$ of $v = x$ and $u = 0$. Then ϕ is strictly increasing on $[-\sqrt{2}, a)$.*

Proof. Notice that $dv/d\theta = -1/2u - V'(\theta)/v$ is monotonic in u. For a fixed θ, suppose that two solutions crossed the fixed θ plane with the same v coordinate. Then the top solution has a larger u coordinate hence by the monotonicity of $dv/d\theta$ will move to the left of the bottom one as θ increases (see Fig. 15).

Since momentum is an integral of motion between bounces, we can use the momentum manifolds, defined as $p_1 + p_2 = $ constant or in θ, u and v coordinates (eliminating r using the energy equation), the expression

$$\left(\frac{h}{\frac{1}{2}(u^2 + v^2) + V(\theta)} \right)^{1/2} (u(\cos\theta + \sin\theta) + v(\cos\theta - \sin\theta))$$

is constant.

Intersections of momentum manifolds with the left face, are shown in Fig. 16. This relation says that for the initial conditions of ϕ if $|v_1| > |v_2|$,
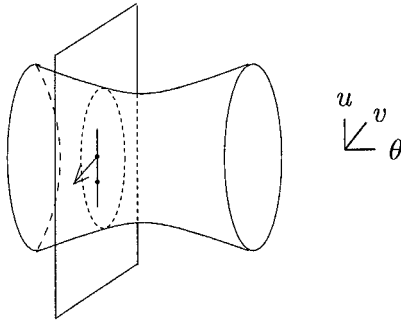
FIG. 15.   Top point must decrease in v faster as u increases.

then the momentum at $v = v_1$, $u = 0$ is greater in magnitude than the momentum at $v = v_2$, $u = 0$. We have chosen initial conditions for ϕ so that if for a fixed θ, two solutions crossed the fixed θ plane with the same v coordinate then the top solution has a larger momentum in absolute value, hence the initial condition for the top solution is to the left of the initial condition for the bottom solution. But we have already noted that the top solution would move to the left of the bottom solution thus preserving monotonicity. ∎

THEOREM 13.2.   *The piece of stable manifold for P_1 with itinerary LRC does not intersect EL.*

Proof.   The endpoints of LRC are LP_2 and LRP_2. From our study of the flow on M, we know that LRP_2 has a positive u-coordinate (see Theorem 7.1). We also know that the endpoints of LRC are to the left of LC. Since LC and LRC are pieces of stable manifold for P_1, they cannot intersect. Therefore all of LRC is to the left of LC.

Above $u = 0$, LC is left of EL. Therefore if LRC and EL did intersect, any point of intersection would have to have a negative u-coordinate. Thus, it is enough to show that LRC is above the line $u = 0$ (see Fig. 17).
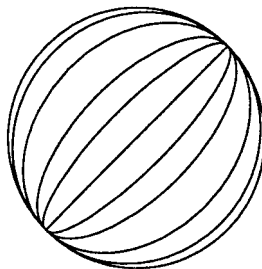
FIG. 16.   Intersection of momentum manifolds and the left face as seen from inside M.
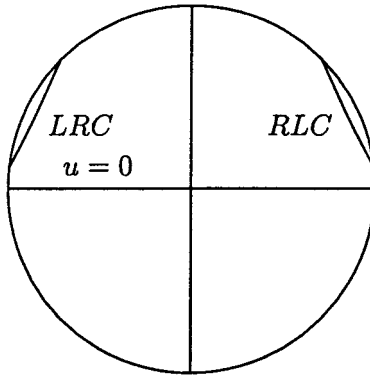
FIG. 17.   The arc *LRC* is above the line $u = 0$.

To see that *LRC* is above $u = 0$, we map both *LRC* and the portion of
the line $u = 0$ described in Lemma 13.1 (see Fig. 17), under $\wp$. The arc
LRC maps to the top part of *RC* and its right-most point is at $v = 1$ and
$u = 1$. By Lemma 13.1 the v coordinates of points on the line $u = 0$ which
cross to the right face are strictly increasing. The left-most point of the
image is at $v = 1$ and $u = -1$ (see Fig. 18). Since the images under $\wp$ of
LRC and $u = 0$ do not intersect, neither do *LRC* and $u = 0$.   ∎

By symmetry both *RLC* and *LRC* are above $u = 0$ and do not cut *EL*
and *ER*. These two curves are pulled back to *LRLC* and *RLRC*.

Recall that the bottom portion of *LC* pulls back to *LLC* and the bottom
portion of *RC* pulls back to *RRC*. Since *RRC* and *LLC* lie above *LC* and
RC, they must cut *EL* and *ER* (see Fig. 19). The top portion of *LLC* is
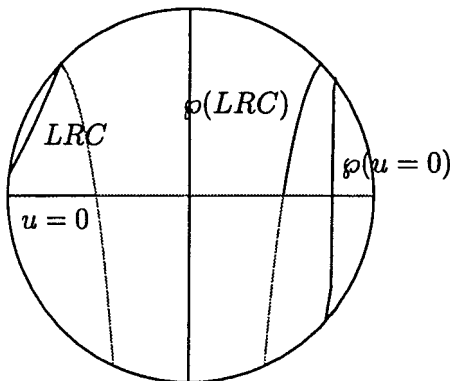
FIG. 18.   The image of *LRC* and the part of $u = 0$ which crosses from left to right.
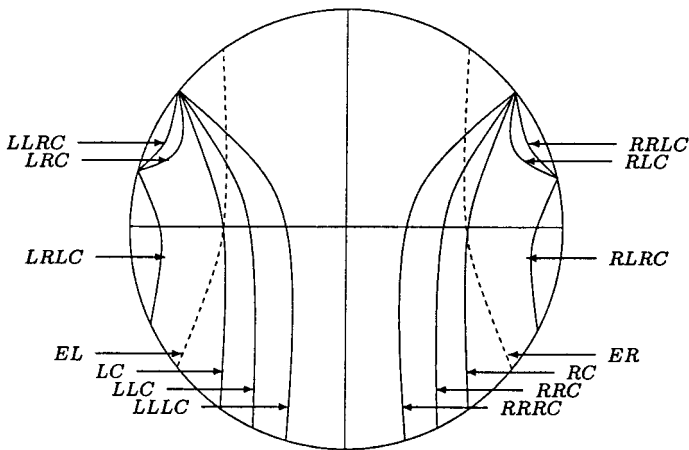
FIG. 19. Caricature of first and second pullbacks of *LC* and *RC*.

pulled back to *RLLC* which has the same end points as *RLRC* but is closer
to the boundary of Σ. Likewise for *LRRC*. The bottom portion of *LLC* is
pulled back to the same side as *LLLC*. The bottom point of *LLLC* is below
the bottom point of *LLC*. Likewise for *RRRC*. For the next pullback, it is
clear that the curves *LRRC* and *RLLC* do not intersect *EL* and *ER*. It is
also clear that *LLLC* and *RRRC* do intersect *EL* and *ER*. It is not clear
if *RLRC* and *LRLC* intersect *EL* and *ER*.

THEOREM 13.3. *The piece of stable manifold for P_1 with itinerary LRLC
does not intersect EL.*

Proof. By Theorem 13.2, *LRC* is above $u = 0$. By the reversibility the
curve *ERL* is below $u = 0$ so *LRC* and *ERL* do not intersect. By mirror
symmetry, *RLC* and *ELR* do not intersect. Since *RLC* and *ELR* do not
intersect, their pre-images under $\wp$, *LRLC* and *EL*, do not intersect. ∎

By symmetry both *RLRC* and *LRLC* intersect neither *EL* nor *ER*. These
two curves are pulled back to *LRLRC* and *RLRLC*. The endpoints of
LRLRC lie on either side of *EL* and so by continuity must intersect *EL* at
least once.

It is not necessary to verify that *LRLRC* and *EL* intersect exactly once.
If they did intersect more that once, loops would form and move around
in the regions as described in Theorem 13.4, not affecting the description of
allowed itineraries. Were loops to form then given some allowed finite
itinerary, there might be several regions which achieve this itinerary. To
keep track such loops would be a very difficult task as is pointed out in
Mayer and Wang [2] (see figure).

THEOREM 13.4. *The set of allowed itineraries in the one-bumper two-body problem with equal masses is described by the sub-shift of finite-type with the restriction of only finite repetitions of L or R.*
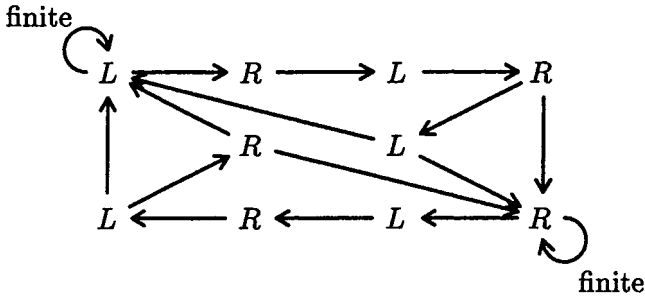
Proof.   Using the pieces of stable and unstable manifold for triple-collision with itineraries *ER*, *EL*, *RC*, *LC*, *RLC*, *LRC*, *RLRC*, *LRLC*, *RLRLC* and *LRLRC* we cut Σ into sixteen regions numbered 1 through 16 as in Fig. 20.

Region 1 is bounded by *M* and *LRC* (see Fig. 20). Region 2 is bounded by *M* and *LRLC*. Region 3 is bounded by *M*, the left portion of *LRLRC* and the bottom portion of *EL*. Region 4 is bounded by *M*, the right portion of *LRLRC* and the bottom portion of *EL*. Region 5 is bounded by the top half of *LC*, *LRC*, *LRLC*, the left portion of *LRLRC* and the middle portion of *EL*. Region 6 is bounded by the top half of *LC* and the top portion of *EL*. Region 7 is bounded by *M*, the bottom half of *LC*, the middle portion of *EL* and the right portion of *LRLRC*. Region 8 is bounded
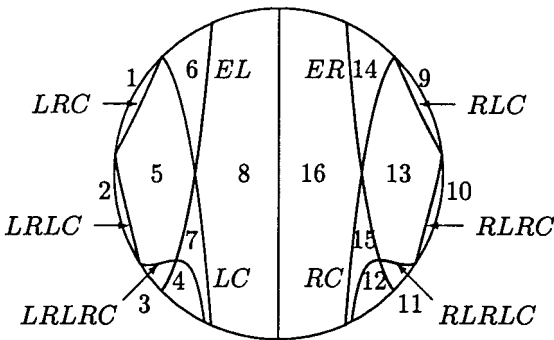
FIG. 20.   Regions of Σ for Theorem 13.4.

above and below by M, by the top portion of EL and the bottom half of LC. Regions 9 through 16 are bounded similarly.

With this partition, we can show how each region maps in backwards time, that is we can find its pre-image under $\wp$. First, we note that the curve EL in backwards time must map to P_2 and so points near EL must leave a neighborhood of P_2 along its one-dimensional stable manifold on M. The bottom point of $EL(P_1L)$ is on the one-dimensional unstable manifold of P_1 so points nearby likewise pull back to the stable manifold of P_1, triple-collision, i.e. LC and RC.

We can now pull back each region and see how these pullbacks stretch over the regions. Let us go through several examples carefully. Region 1 is bounded by M and LRC. By Theorem 13.2, LRC does not intersect EL so it pulls back to $RLRC$. So, region 1 pulls back to region 10.
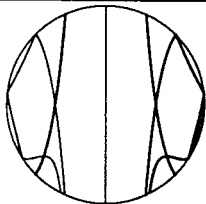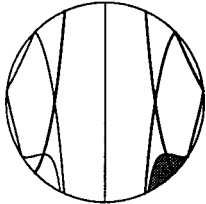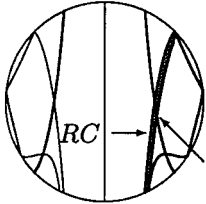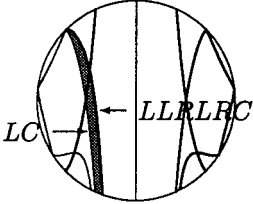
Region	Preimage Under $\wp$	
1	all of 10	
2	all of 11 and 12	
3	across 13 and 15	
4	across 6 and 8	

FIG. 21. Preimages of the left regions 1 to 4.
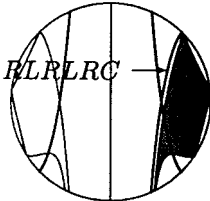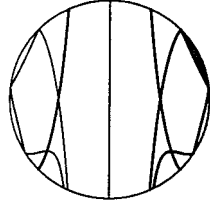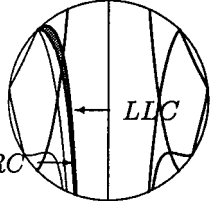
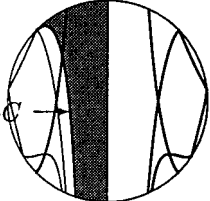| Region	Preimage Under $\wp$
5	across 13 and 15
6	all of 9
7	across 6 and 8
8	across 6 and 8

Fig. 22.   Preimages of the left regions 5 to 8.
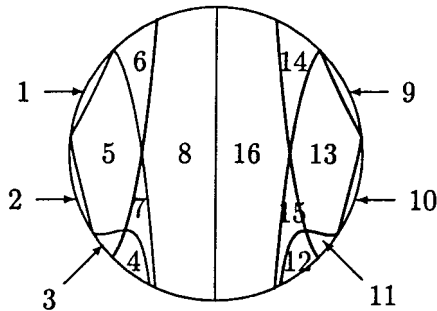

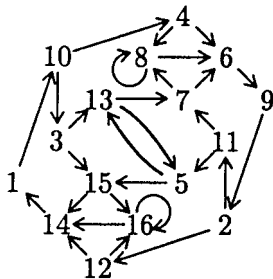Fig. 23.   Regions of Σ for Theorem 13.4.

FIG. 24.   Directed graph describing how the regions move under preimages of $\wp$.

Region 2 is bounded by M and $LRLC$. By Theorem 13.3, $LRLC$ does not intersect EL so it pulls back to $RLRLC$. So, region 2 pulls back to all of regions 11 and 12.

Region 3 is bounded by M, the left portion of $LRLRC$ and the bottom portion of EL. The left portion of $LRLRC$ pulls back to $RLRLRC$. A small neighborhood of the bottom point of $EL(P_1L)$ in region 3 pulls back to a neighborhood of RC so RC is a boundary of the pre-image of region 3. So, the pre-image of region 3 is a wedge that cuts across regions 13 and 15.

Region 4 is bounded by M, the right portion of $LRLRC$ and the bottom portion of EL. The right portion of $LRLRC$ pulls back to $LLRLRC$. A small neighborhood of the bottom point of EL in region 4 pulls back to a neighborhood of LC so LC a boundary of the pre-image of region 4. So, the pre-image of region 4 is a wedge that cuts across regions 6 and 8.

By continuing to analyze the pullbacks of the boundaries of each region, we can say how each region pulls back (see Figs. 21–23). Region 5 must map across 13 and 15. Region 6 must map to region 9. Finally, regions 7 and 8 must each map across both 6 and 8. By symmetry, we can construct a directed graph to describe how all the regions interact. (Fig. 24).

We can reduce the graph in Fig. 24. That is, regions 3 and 5 each map onto (different parts of) the same regions. This means that regions 3 and 5 can be combined into a new region $3'$. By symmetry, regions 11 and 13
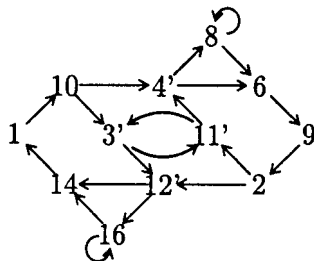

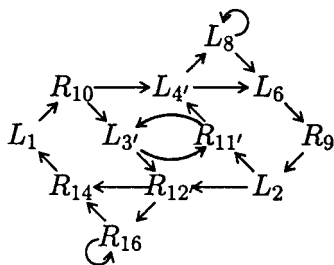FIG. 25.   Directed graph for reduced regions.

FIG. 26.   Directed graph using left and right bounce symbols.

can be combined into a new region 11′. Since regions 4 and 7 map onto (different parts of) the same regions, regions 4 and 7 can be combined into 4′. Likewise, regions 12 and 15 can be combined into 12′. This yields the graph in Fig. 25.

We can replace each number in the new graph by which bounce each region corresponds to, L or R. This yields the graph in Fig. 26.

Assume for example that we have some string of three or more right bounces, then we must be at R_{16}. The only way to leave for another region is $R_{14} \to L_1 \to R_{10}$. What follows next must be a left bounce. If it is through $L_{4'}$, then it is possible to have a string of two or more left bounces. If it is through $L_{3'}$ then the next bounce must be on the right. However, after that right can be a long string of lefts ($L_{3'} \to R_{11'} \to R_{4'}$), a single left followed by a right ($L_{3'} \to R_{11'} \to R_{3'}$), or a long string of rights ($L_{3'} \to R_{12'}$). This gives rise to the diagram in Fig. 27.

By symmetry, we get the diagram stated in the Theorem.

The infinite strings are omitted since initial conditions can be chosen in the interior of the phase space close enough to S_2^l and S_2^r so that its itinerary begins with a sequence of L's or R's of arbitrary but finite length. The limiting case is on the collision manifold or along $v = 0$ and $\theta = \pi/2$ or π, which are fixed by the identification at binary collisions.

Using our partition of the left and right faces we have shown that any allowed itinerary can be generated by the directed graph in stated in the
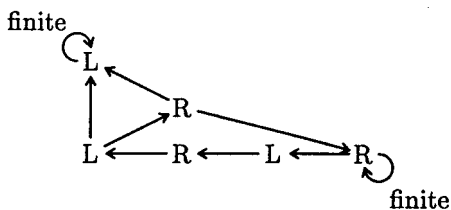

FIG. 27.   Analysis of Fig. 26.

Theorem. We next show that the converse is true, that is, the map from orbits to itineraries is onto the set of itineraries allowed by the directed graph in stated in the Theorem.

For each (reduced) region we draw a schematic square whose four sides correspond to the region's boundaries (see Fig. 28). With the orientation induced by the square, we see that vertical strips pull back to vertical strips. If a region has two pre-images, we see that a vertical strip pulls back to a vertical strip stretched across both pre-images (see Fig. 29). The reader is referred to Figs. 21 and 22.

In region 1, a strip from LP_2 to LRP_2 pulls back to a strip from RLP_2 to $RLRP_2$ in region 10.

In region 2, a strip from LRP_2 to $LRLP_2$ pulls back to a strip from M (including the point $RLRP_2$) to ER in region 11′ and to a strip from ER to M (including the point $RLRLP_2$) in region 12′.

In region 3′, a strip from M to EL pulls back to a strip from RP_2 to ER in region 11′ and to a strip from EL to M in region 12′. A strip from M to LRP_2 pulls back to a strip from M (including the point $RLRP_2$) to EL in region 11′ and to a strip from EL to M in region 12′. A strip from LP_2 to EL pulls back to a strip from RP_2 to RLP_2 in region 11′. A strip from LP_2 to LRP_2 pulls back to a strip from M (including the point $RLRP_2$) to RLP_2 in region 11′.
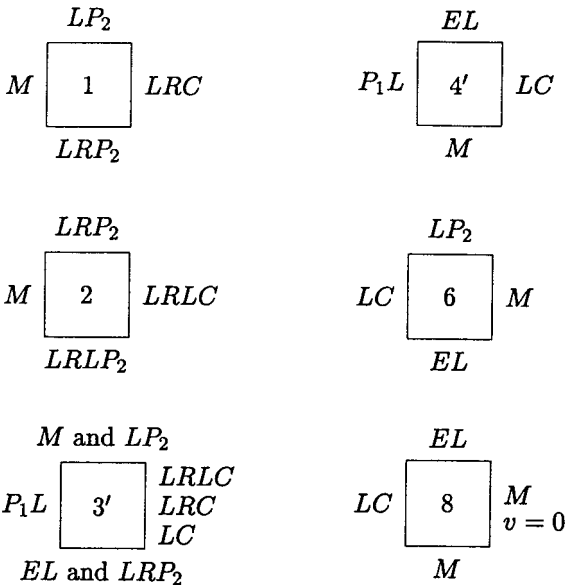

FIG. 28. Schematic of regions on the left face. Schematics for the regions on the right face are symmetric to these.
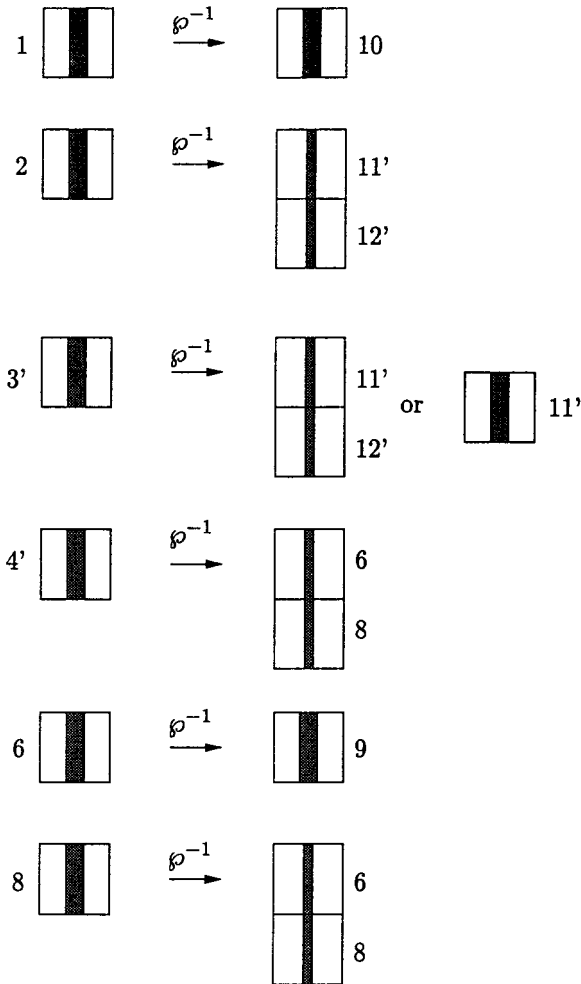
FIG. 29.   Pullbacks of vertical strips in regions of the left face. See also Figs. 21 and 22.

In region 4′, a strip from EL to M pulls back to a strip from LP_2 to EL in region 6 and to a strip from EL to M in region 8.

In region 6, a strip from LP_2 to EL pulls back to a region from RP_2 to LRP_2 in region 9.

In region 8, a strip from EL to M maps to a strip from LP_2 to EL in region 6 and from EL to M in region 8.

Given any itinerary allowed by the directed graph given in the Theorem, there exists at least one corresponding sequence of regions in the directed graph in Fig. 25. Taking a vertical strip in the initial region, we pull back

according to the given sequence. At the nth pullback, there is a non-empty closed set within the initial vertical strip which pulls back to the nth region. Taking the limit, we have a nested intersection of closed sets which is non-empty. So there is at least one point which attains the given itinerary in backward time. We now apply reversibility to such an initial condition and achieve a point which attains the given itinerary in forward time. ∎

It is important to keep in mind that we only have a semi-conjugacy to a sub-shift of finite type in Theorem 13.4. In fact, numerically there is an elliptic periodic point along $u = 0$ whose itinerary is *LRLR...*. If this periodic point is elliptic (which we do not attempt to prove), all the points in a small region about this periodic point also have the itinerary *LRLR...* even though they are not necessarily periodic under $\wp$.

14. CONCLUDING REMARKS

One interpretation of Theorem 13.4 is that if a mass bounces two or more times in a row then for the next bounce to be on the other side of the bumper means that the solution has come close enough to triple collision that it follows the flow on the collision manifold for at least a short time. The flow on the collision manifold dictates that the next three bounces must alternate. This, then, is the global effect of the presence of the triple-collision manifold on the dynamics of the model. That is, the triple-collision manifold excludes certain sequences by virtue of continuity. One expects that a similar mechanism in the collinear three-body problem restricts the global dynamics.

We also expect that a finite representation of allowed orbits in the collinear three-body problem is possible. To see why, let us look more closely at our model. In Theorem 13.4 we chose sixteen regions on the Poincaré slice bounded by pieces of stable and unstable manifold for triple collision. There are many more regions we could have chosen (see Fig. 19). Any other region we generate will be a subset of one of the sixteen and will split under pullbacks at the same time as the larger region. Therefore any smaller region has redundant information about what sequences are allowed.

To generate the sixteen regions we actually asked the question how many pullbacks of the top half of *LC* (or *RC*) are required for it to intersect *EL* or *ER*. It is exactly these pullbacks and *EL* and *ER* which form the boundaries of the sixteen regions. Any bifurcations which occur by changing masses happen exactly when the required number of pullbacks of *LC* to intersect *EL* or *ER* changes. Such a strategy for studying the allowed dynamics and bifurcations of the collinear three-body problem might be fruitful.

ACKNOWLEDGMENTS

REFERENCES

1. Richard McGehee, Triple collision in the collinear three-body problem, *Invent. Math.* **27** (1974), 191–227.
2. K. R. Meyer and Q. D. Wang, The collinear three-body problem with negative energy, *J. Differential Equations*, in press.
3. Henri Poincaré, Sur les problèmes des trois corps et les équations dynamiques, *Acta Math.* **13** (1890).